Published in final edited form as:
Phys Chem Chem Phys. 2012 July 21; 14(27): 9654–9659. doi:10.1039/c2cp41207a.

Improvement of durability of an organic photocatalyst in *p*-xylene oxygenation by addition of a Cu(II) complex†

Yusuke Yamada[a], **Kazuki Maeda**[a], **Kei Ohkubo**[a], **Kenneth D. Karlin**[*,b,c], and **Shunichi Fukuzumi**[*,a,c]

[a]Department of Material and Life Science, Division of Advanced Science and Biotechnology, Graduate School of Engineering, Osaka University, ALCA, Japan Science and Technology Agency (JST), Suita, Osaka 565-0871, Japan

[b]Department of Chemistry, The Johns Hopkins University, Baltimore, MD 21218, USA

[c]Department of Bioinspired Science, Ewha Womans University, Seoul 120-750, Korea

Abstract

The catalytic durability of an organic photocatalyst, 9-mesityl-10-methyl acridinium ion (Acr^+–Mes), has been dramatically improved by the addition of [{tris(2-pyridylmethyl)amine}-Cu^{II}]$(ClO_4)_2$ ([(tmpa)Cu^{II}]$^{2+}$) in the photocatalytic oxygenation of *p*-xylene by molecular oxygen in acetonitrile. Such an improvement is not observed by the addition of $Cu(ClO_4)_2$ in the absence of organic ligands. The addition of [(tmpa)Cu]$^{2+}$ in the reaction solution resulted in more than an 11 times higher turnover number (TON) compared with the TON obtained without [(tmpa)Cu^{II}]$^{2+}$. In the photocatalytic oxygenation, a stoichiometric amount of H_2O_2 formation was observed in the absence of [(tmpa)Cu^{II}]$^{2+}$, however, much less H_2O_2 formation was observed in the presence of [(tmpa)Cu^{II}]$^{2+}$. The photocatalytic mechanism was investigated by laser flash photolysis measurements in order to detect intermediates. The reaction of $O_2^{\cdot-}$ with [(tmpa)Cu^{II}]$^{2+}$ monitored by UV-vis spectroscopy in propionitrile at 203 K suggested formation of [{(tmpa)Cu^{II}}$_2O_2$]$^{2+}$, a transformation which is crucial for the overall 4-electron reduction of molecular O_2 to water, and a key in the observed improvement in the catalytic durability of Acr^+–Mes.

1. Introduction

A variety of organic reactions such as oxygenation, carbon–carbon bond formation and polymerization, have been accomplished by employing heavy transition metal catalysts,[1,2] however, the increased attention on environmental problems demands a focus toward alternative and more environmentally benign methods.[3,4] Recently, utilization of organic catalysts has been regarded as a promising method to avoid such problems because of their environmentally benign character. Especially, the employment of organic photocatalysts utilizing visible light has attracted many researchers expecting to produce products which are difficult to obtain *via* thermal reactions.[5–7]

Among such photocatalysts, a donor–acceptor linked dyad has been regarded as a prominent catalyst because of its already proven wide variety of applications.[8–14] For example, oxidation of benzene to phenol where the oxygen atom derives from water as its source has

†Electronic supplementary information (ESI) available: UV-vis spectra of titration of H_2O_2 with NaI in MeCN (Fig. S1).

*fukuzumi@chem.eng.osaka-u.ac.jp, karlin@jhu.edu; Fax: +81-6-6879-7370; Tel: +81-6-6879-7368.

been made possible without producing further oxygenated compounds.[15,16] Bromination of various aromatic compounds has also been achieved without using toxic bromine.[17] The donor–acceptor linked dyad can be also utilized in the oxygenation of aromatic compounds to produce aromatic aldehydes,[18] which is a key chemical reaction for the production of precursors of a variety of fine or speciality chemicals such as pharmaceutics, organic dyes, pesticides and perfumes.[19–24]

9-Mesityl-10-methylacridinium ion (Acr^+–Mes)[9,10] and its derivatives have been reported to act as efficient photocatalysts for oxygenation of toluene derivatives to corresponding aldehydes in photocatalytic oxygenation under visible light irradiation.[18] The electron-transfer state ($Acr^{\cdot}$–$Mes^{\cdot+}$), produced upon photoexcitation of Acr^+–Mes, has both strong oxidizing and reducing ability, and this enables it to not only oxidize alkyl aromatic compounds but also to reduce O_2.[10,14] However, the accompanying formation of reactive oxygen species (ROS) may be problematic, because they may irreversibly oxidize the organic photocatalyst leading to its deactivation.

Organic catalyst durability is highly desirable for practical applications, especially in oxygenation reaction systems. In a previous report, the turnover number of an organic photocatalyst of Acr^+–Mes was lower than 100 in the oxygenation of *p*-xylene by O_2 using Acr^+–Mes as a photocatalyst. Without a substrate, Acr^+–Mes itself is oxidized by O_2 under photoirradiation.[25] The ROS $O_2^{\cdot-}$ can be produced by electron transfer from the $Acr^{\cdot}$ moiety of the photogenerated electron-transfer state ($Acr^{\cdot}$–$Mes^{\cdot+}$) to O_2, and this may be responsible for the oxidation of the photocatalyst. Yet $O_2^{\cdot-}$ is known to be efficiently trapped by various metal ions including Cu(II) complexes; Cu–O_2 complexes have recently been extensively investigated.[26–29] Thus, our thinking was that the presence of a copper complex in oxygenation reaction systems might improve organic catalyst durability and the reaction mechanism might be clarified by spectroscopic detection of a Cu–O_2 intermediate.

We herein report a significant improvement of the photocatalytic durability of Acr^+–Mes in the selective oxygenation of *p*-xylene with O_2 by the addition of [{tris(2-pyridylmethyl)-amine}Cu^{II}]$(ClO_4)_2$ ([(tmpa)Cu^{II}]$^{2+}$).[26–29] This Cu complex is expected to efficiently react with $O_2^{\cdot-}$,[28,29] the latter is likely a significant product of O_2-reduction. For comparison, $Cu(ClO_4)_2$ was added to the reaction solution but found to not be useful. Spectroscopic studies using nanosecond laser flash photolysis and UV-vis absorption at low temperature have enabled us to clarify the role of [(tmpa)Cu^{II}]$^{2+}$ and to propose a mechanism for the significantly improved photocatalytic durability of the Acr^+–Mes catalyst.

2. Experimental section

9-Mesityl-10-methylacridinium perchlorate [(Acr^+–Mes)(ClO_4)] was purchased from Tokyo Chemical Industry and recrystallized from absolute ethanol before use. *p*-Xylene was obtained from Wako Pure Chemicals. Copper(II) perchlorate hexahydrate and tris(2-pyrydylmethyl)amine were purchased from Nacalai tesuque and Tokyo Chemical Industry, respectively. Purified water was provided by a Millipore MilliQ water purification system where the electronic conductance was 18.2 MΩ cm.

2.1. Synthesis of $[Cu^{II}(tmpa)](ClO_4)_2$

$[Cu^{II}(tmpa)](ClO_4)_2$ was synthesized by the reported method.[30] Copper(II) perchlorate hexahydrate (131 mg, 0.035 mmol) was slowly added to an acetonitrile (MeCN) solution (4.0 mL) of tris(2-pyridylmethyl)amine (100 mg, 0.035 mmol). The deep blue solution obtained was stirred for 30 min at room temperature and then ether (10 mL) was slowly added to precipitate blue powder which was collected by filtration and recrystallized from

MeCN and diethyl ether (Yield 155 mg, 75%). Anal. Calcd. for $C_{20}H_{21}Cl_2CuN_5O$: C, 40.45; H, 3.56; N, 11.79. Found; C, 40.36; H, 3.32; N, 11.68.

2.2. Photocatalytic *p*-xylene oxygenation

The photocatalytic oxygenation of *p*-xylene was carried out by the following procedure. Typically, an MeCN solution (0.6 mL) containing (Acr^+–Mes)(ClO_4) (2.0×10^{-4} M), *p*-xylene (3.0×10^{-2} M) and [(tmpa)Cu^{II}](ClO_4)$_2$ in a quartz glass tube (i.d. 5 mm) with a rubber septum was saturated with oxygen by bubbling pure oxygen through a stainless steel needle for 5 min. The solution was then irradiated with a 500 W xenon lamp (Ushio Optical ModelX SX-UID 500XAMQ) through a colour filter glass (Asahi Techno Glass, $\lambda > 390$ nm) at 298 K. After photoirradiation, the solution was analysed periodically by ^{1}H NMR spectroscopy (JEOL JNM-AL300 spectrometer) to identify and quantify the products. The amount of H_2O_2 formed was determined by titration by iodide ion; the diluted reaction mixture was treated with an excess amount of NaI in MeCN. The concentration of I_3^- formed was then determined from the UV-vis spectrum (λ_{max} = 361 nm, $\varepsilon = 2.50 \times 10^4$ M^{-1} cm^{-1} in MeCN).[31] The yield of H_2O_2 was also determined by ^{1}H NMR spectroscopy. H_2O_2: ^{1}H NMR (CD_3CN): 8.67 (s, 2H).

2.3. Time-resolved absorption spectral measurements

For nanosecond laser flash photolysis experiments, an MeCN solution (2.0 mL) containing (Acr^+–Mes)(ClO_4) and [(tmpa)Cu^{II}](ClO_4)$_2$ was deaerated by bubbling N_2 for 10 min. Then, a certain amount of O_2-saturated MeCN was added to the deaerated reaction solution. Then the mixed solution was photoirradiated by an Nd:YAG laser (Continuum, SLII-10, 4–6 ns fwhm) at λ = 430 nm with the power of 3.6 mJ per pulse. The transient absorption measurements were performed using a continuous xenon lamp (150 W) as a probe light and a photomultiplier (Hamamatsu R2949; 350–800 nm) as a detector, respectively.

2.4. UV-vis absorption spectroscopy under photoirradiation at low temperature

An O_2-saturated propionitrile (EtCN) solution containing 1-benzyl–1,4-dihydronicotinamide dimer (0.25 mM), (Acr^+–Mes)(ClO_4) (0.050 mM) and [Cu^{II}(tmpa)](ClO_4)$_2$ (0.50 mM) was cooled in a quartz cuvette (light path length: 1.0 cm) to 203 K. UV-vis spectra were taken after photoirradiation (λ = 430 nm).

3. Results and discussion

3.1. *p*-Xylene oxygenation catalysed by Acr^+–Mes in the presence of [(tmpa)Cu^{II}]$^{2+}$

The photocatalytic *p*-xylene oxygenation using molecular oxygen was performed by photoirradiation ($\lambda > 390$ nm) of a deuterated MeCN solution using Acr^+–Mes as a photocatalyst in the absence and presence of [(tmpa)Cu^{II}]$^{2+}$. The oxygenation of *p*-xylene resulted in conversion to *p*-tolualdehyde and H_2O_2 (eqn (1)). Fig. 1 shows a typical ^{1}H NMR

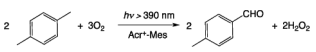

(1)

spectrum of the solution during the reaction. The ^{1}H NMR spectroscopic signals assigned to *p*-xylene appeared around 2.6 ppm (CH_3 group) and 7.0 ppm (phenyl ring) and those assigned to *p*-tolualdehyde appeared around 2.7 ppm (CH_3 group), 7.3 ppm and 7.8 ppm (phenyl group) and 9.9 ppm (aldehyde). No overlapping of peaks of the reactant and product assures that the quantification by ^{1}H NMR is reliable in this reaction system. The ^{1}H NMR peaks assignable to Acr^+–Mes were negligible due to its relatively low concentration ($2.0 \times$

10^{-4} M). Formation of *p*-methylbenzyl alcohol is possible during the oxygenation as an intermediate, however, none of this product was observed in any significant amount when in the presence of $[(tmpa)Cu^{II}]^{2+}$.

The time profiles of *p*-tolualdehyde and H_2O_2 yields in this photooxygenation with different concentrations of $[(tmpa)Cu^{II}]^{2+}$ are shown in Fig. 2. In the absence of $[(tmpa)Cu^{II}]^{2+}$, the yields of *p*-tolualdehyde and H_2O_2 reached 30% and 26% with photoirradiation for 3.5 h, respectively. The similarity of yields assures that the oxygenation proceeded following eqn (1). The yield of *p*-tolualdehyde increased with increasing concentrations of $[(tmpa)Cu^{II}]^{2+}$ up to 2.0 mM to reach a constant value of 57% in 3.5 h, which is nearly double the yield achieved in the absence of $[(tmpa)Cu^{II}]^{2+}$. On the other hand, the H_2O_2 yield decreased from 26% achieved in the absence of $[(tmpa)Cu^{II}]^{2+}$ to 5% in the presence of 2.0 mM $[(tmpa)Cu^{II}]^{2+}$. A separate experiment involving reaction of $[(tmpa)Cu^{II}]^{2+}$ with H_2O_2 was conducted to confirm whether or not $[(tmpa)Cu^{II}]^{2+}$ catalyzed the decomposition of H_2O_2 produced. No significant change in H_2O_2 concentration was detected by iodometry, as shown in Fig. S1 in the ESI.† Thus, the reaction mechanism of the O_2 reduction appears to be altered in the presence of $[(tmpa)Cu^{II}]^{2+}$. On the other hand, the quantum yield for the photocatalytic oxidation of *p*-xylene in the presence of $[(tmpa)Cu^{II}]^{2+}$ (1.0 mM), Acr^+–Mes (2.0×10^{-4} mM) and *p*-xylene (1.0×10^{-2} M) excited at 420 nm was determined to be 0.13 using ferrioxalate actinometer. The quantum yield was similar to that determined for the reaction system in the absence of $[(tmpa)Cu^{II}]^{2+}$.[18]

Fig. 3a shows the UV-vis absorption spectra of the reaction solutions with different concentrations of $[(tmpa)Cu^{II}]^{2+}$ after photoirradiation for 3.5 h alongside a solution not undergoing photoirradiation. The characteristic bands of Acr^+–Mes around 360 nm and 423 nm decreased after photoirradiation, indicating the decomposition of Acr^+–Mes during the reaction. Fig. 3b shows the survival ratio of Acr^+–Mes estimated from the relative absorbance at 423 nm depending on the reaction solution concentration of $[(tmpa)Cu^{II}]^{2+}$. The survival ratio of Acr^+–Mes increased in proportion to the concentration of $[(tmpa)Cu^{II}]^{2+}$ up to 0.5 mM reaching a high of 78%.

The high survival ratio of Acr^+–Mes in the presence of $[(tmpa)Cu^{II}]^{2+}$ also benefits the turnover number (TON) in the photooxygenation of *p*-xylene. Fig. 4 shows the time profiles of the TON for the photocatalytic *p*-xylene oxidation in MeCN. These experiments were performed by photoirradiation of an MeCN solution containing *p*-xylene (6.0×10^{-2} M) and Acr^+–Mes (2.0×10^{-4} M) in the absence or presence of $[(tmpa)Cu^{II}]^{2+}$ (2.0×10^{-3} M). In the absence of $[(tmpa)Cu^{II}]^{2+}$, the TON of Acr^+–Mes reached ~100 although the ratio of *p*-xylene to Acr^+–Mes was 300, indicating the deactivation of Acr^+–Mes during the reaction. In the presence of $[(tmpa)Cu^{II}]^{2+}$, *p*-xylene in the reaction solution was completely converted to *p*-tolualdehyde. When *p*-xylene (3.6×10^{-5} mol) was further added to the reaction solution after this photoirradiation, it was also completely converted to *p*-tolualdehyde, in this second round. For three additions of *p*-xylene, its complete conversion was observed. Thus, the TON of Acr^+–Mes in the presence of $[(tmpa)Cu^{II}]^{2+}$ became higher than 1200, which is more than 11 times higher than the TON obtained without $[(tmpa)Cu^{II}]^{2+}$. In contrast to the case of $[(tmpa)Cu^{II}]^{2+}$, a significant deceleration was observed in the *p*-xylene oxygenation reaction with the addition of $Cu^{II}(ClO_4)_2$.

†Electronic supplementary information (ESI) available: UV-vis spectra of titration of H_2O_2 with NaI in MeCN (Fig. S1).

3.2. Kinetic studies of electron transfer from photogenerated $Acr^{\cdot}$–$Mes^{\cdot+}$ to O_2 and $[(tmpa)Cu^{II}]^{2+}$

Nanosecond laser flash photolysis measurements on Acr^+–Mes were conducted to detect the electron-transfer state ($Acr^{\cdot}$–$Mes^{\cdot+}$) in the absence and presence of O_2 and $[(tmpa)Cu^{II}]^{2+}$. Laser excitation at 430 nm of an MeCN solution containing Acr^+–Mes (1.0×10^{-4} M) results in the formation of the electron-transfer state ($Acr^{\cdot}$–$Mes^{\cdot+}$).[7,32] Fig. 5a shows the decay curves of absorption at 500 nm due to the $Acr^{\cdot}$ moiety of $Acr^{\cdot}$–$Mes^{\cdot+}$. The absorption decay became faster by increasing the concentration of O_2 in the solution. The decay obeyed pseudo-first-order kinetics and the pseudo-first-order rate constant (k_{obs}) increased linearly with increasing concentration of O_2, as shown in Fig. 5b. The second-order rate constant (k_{O_2}) of electron transfer from the $Acr^{\cdot}$ moiety of $Acr^{\cdot}$–$Mes^{\cdot+}$ to O_2 was determined from the slope of a linear plot in Fig. 5b to be 6.5×10^8 M^{-1} s^{-1}. The presence of $[(tmpa)Cu^{II}]^{2+}$ also increased the decay rate of the $Acr^{\cdot}$ moiety of $Acr^{\cdot}$–$Mes^{\cdot+}$ generated by photoirradiation. The decay rate also obeyed pseudo-first-order kinetics and the pseudo-first-order rate constant (k_{obs}) increased linearly with increasing concentration of $[(tmpa)Cu^{II}]^{2+}$, as shown in Fig. 5d. The second-order rate constant (k_{Cu}) of electron transfer from $Acr^{\cdot}$–$Mes^{\cdot+}$ to $[(tmpa)Cu^{II}]^{2+}$ was determined to be 1.5×10^8 M^{-1} s^{-1} from the slope of the plot shown in Fig. 5d. The smaller second-order rate constants of k_{Cu} compared with k_{O_2} confirms that the electron transfer from the $Acr^{\cdot}$ moiety of $Acr^{\cdot}$–$Mes^{\cdot+}$ to $[(tmpa)Cu^{II}]^{2+}$ is much slower than that to O_2 under the present reaction conditions, because the concentration of O_2 is 13 mM, which is more than 5 times higher than the concentration of $[(tmpa)Cu^{II}]^{2+}$.

3.3. Detection of reaction intermediate at low temperature

The kinetic measurements suggest that the one-electron reduction of O_2 by the $Acr^{\cdot}$ moiety occurred in both the absence and presence of $[(tmpa)Cu^{II}]^{2+}$. In the absence of $[(tmpa)Cu^{II}]^{2+}$, H_2O_2 was formed by disproportionation of two molecules of $O_2^{\cdot-}$, which is formed by the one-electron reduction of O_2 with the $Acr^{\cdot}$ moiety. Thus, the lesser formation of H_2O_2 in the presence of $[(tmpa)Cu^{II}]^{2+}$ suggests that $O_2^{\cdot-}$ may react with $[(tmpa)Cu^{II}]^{2+}$ before the disproportionation. The intermediate species can be detected in the presence of 1-benzyl-1,4-dihydronicotinamide dimer $[(BNA)_2]$, which acts as a two-electron donor to be able to reduce O_2 to two equivalents of $O_2^{\cdot-}$.[33,34]

The UV-vis spectral change was recorded for an EtCN solution containing $(BNA)_2$ (2.5×10^{-4} M), Acr^+–Mes (5.0×10^{-5} M) and $[(tmpa)Cu^{II}]^{2+}$ (5.0×10^{-4} M) by photoirradiation ($\lambda = 420$ nm) at 203 K as shown in Fig. 6a. Characteristic absorption bands around 525 nm and 610 nm assignable to $[\{(tmpa)Cu^{II}\}_2O_2]^{2+}$ complex[26–29] increased while the absorption around 410 nm owing to $(BNA)_2$ decreased with photoirradiation. Time profiles of the absorbance at 410 nm and 525 nm are indicated in Fig. 6b. These clearly showed the oxidation of $(BNA)_2$ and formation of $[\{(tmpa)Cu^{II}\}_2O_2]^{2+}$ in the same time regime.

When $Cu(ClO_4)_2$ was used instead of $[(tmpa)Cu^{II}]^{2+}$, neither the appearance of absorption around 520 nm nor the decay of absorbance at 410 nm was observed (Fig. 7). The photoirradiation of Acr^+–Mes results in the formation of $Acr^{\cdot}$–$Mes^{\cdot+}$ and the $Acr^{\cdot}$ moiety of $Acr^{\cdot}$–$Mes^{\cdot+}$ reduces O_2 to produce $O_2^{\cdot-}$ and Acr^+–$Mes^{\cdot+}$.[8] $O_2^{\cdot-}$ may reduce a Cu^{2+} ion to produce a Cu^+ ion and O_2, and the Cu^+ ion may be immediately oxidized by the $Mes^{\cdot+}$ moiety of Acr^+–$Mes^{\cdot+}$ to regenerate Acr^+–Mes and a Cu^{2+} ion. Thus, the back electron transfer from Cu^+ to the $Mes^{\cdot+}$ moiety of Acr^+–$Mes^{\cdot+}$ prohibits the oxidation of $(BNA)_2$ in EtCN as well as the *p*-xylene substrate in the original reaction solution.

Scheme 1 depicts the derived photocatalytic reaction mechanism with $[(tmpa)Cu^{II}]^{2+}$. The photocatalyst Acr^+–Mes forms the long-lived electron-transfer state $Acr^{\cdot}$–$Mes^{\cdot+}$ following photoirradiation.[7,32] The $Mes^{\cdot+}$ moiety of $Acr^{\cdot}$–$Mes^{\cdot+}$ oxidizes *p*-xylene to a *p*-xylene

radical cation, because the oxidation potential of *p*-xylene (1.93 V *vs.* SCE) is lower than the reduction potential of $Acr^{\cdot -}$–$Mes^{\cdot +}$ (2.06 V *vs.* SCE).[18] Because the one-electron oxidation potential of the product (*p*-tolualdehyde) is also higher than the reduction potential of $Acr^{\cdot}$–$Mes^{\cdot +}$, no further oxidation of *p*-tolualdehyde occurred, making the present photocatalytic oxygenation of *p*-xylene highly selective.[18] Then, the *p*-xylene radical cation formed is immediately deprotonated to produce a *p*-methylbenzyl radical. This carbon-centered radical reacts with molecular oxygen to give the *p*-methylbenzylperoxyl radical, which disproportionates to yield *p*-methylbenzyl alcohol and *p*-tolualdehyde.[16] *p*-Methylbenzyl alcohol is further oxidized by the same catalytic cycle, even more efficiently, to produce *p*-tolualdehyde as the final oxidized product of *p*-xylene.[14,18] On the other hand, the $Acr^{\cdot}$ moiety can react with O_2 as evidenced by nanosecond laser flash photolysis (Fig. 5a). The $O_2^{\cdot -}$ produced reacts with $[(tmpa)Cu^{II}]^{2+}$ to form $[(tmpa)Cu^{II}(O_2^{\cdot -})]^{+}$, which is known to be in equilibrium with $[(tmpa)Cu^{I}]^{+}$ and O_2.[28] The Cu(II)-superoxo complex $[(tmpa)Cu^{II}(O_2^{\cdot -})]^{+}$ is further reduced by $[(tmpa)Cu^{I}]^{+}$ to form the dinuclear Cu(II)-peroxo complex $[\{(tmpa)Cu^{II}\}_2O_2]^{2+}$ as shown in Fig. 6a.[32] The fast trap of $O_2^{\cdot -}$ by $[(tmpa)Cu^{II}]^{2+}$ prevents back electron transfer from $O_2^{\cdot -}$ to the $Mes^{\cdot +}$ moiety of $Acr^{\cdot}$–$Mes^{\cdot +}$, resulting in acceleration of the photocatalytic oxygenation of *p*-xylene with O_2 as shown in Fig. 2a. It was reported that $[\{(tmpa)Cu^{II}\}_2O_2]^{2+}$ was further reduced in the presence of protons to produce H_2O accompanied by regeneration of $[(tmpa)Cu^{II}]^{2+}$.[35] Thus, the formation of H_2O_2 is avoided by the presence of $[(tmpa)Cu^{II}]^{2+}$, which can catalyze the four-electron reduction of O_2 (Fig. 2b).[35] The removal of potential oxidants ($O_2^{\cdot -}$ and H_2O_2) by $[(tmpa)Cu^{II}]^{2+}$ led to improvement of the durability of the photocatalyst (Acr^{+}–Mes) as shown in Figs 3 and 4.

Conclusions

The photocatalytic durability of Acr^{+}–Mes in the selective photocatalytic oxygenation of *p*-xylene with O_2 to yield *p*-tolualdehyde was significantly improved by addition of $[(tmpa)Cu^{II}]^{2+}$; the latter can trap $O_2^{\cdot -}$ produced by the one-electron reduction of O_2 by the $Acr^{\cdot}$ moiety of $Acr^{\cdot}$–$Mes^{\cdot +}$, which is the photoproduct of the organic Acr^{+}–Mes catalyst. Overall, molecular oxygen is reduced to water *via* the dinuclear Cu^{II}-peroxo complex, $[\{(tmpa)Cu^{II}\}_2O_2]^{2+}$. In contrast to the case of $[(tmpa)Cu^{II}]^{2+}$, $Cu^{II}(ClO_4)_2$ prohibits the photocatalytic oxygenation of *p*-xylene with O_2 because of the fast back electron transfer from the Cu^{+} ion to the $Mes^{\cdot +}$ moiety of $Acr^{\cdot}$–$Mes^{\cdot +}$. In conclusion, the efficient trapping of $O_2^{\cdot -}$ by $[(tmpa)Cu^{II}]^{2+}$ and its further reduction to water with $[(tmpa)Cu^{I}]^{+}$ prevents degradation of Acr^{+}–Mes by its oxidation with reactive oxygen species.

Supplementary Material

Refer to Web version on PubMed Central for supplementary material.

Acknowledgments

This work was partially supported by a Grant-in-Aid (Nos. 20108010 and 23750014) and a Global COE program, “the Global Education and Research Centre for Bio-Environmental Chemistry” (to S.F.) from the MEXT, Japan, and NRF/MEST of Korea through WCU (R31-2008-000-10010-0) and GRL (2010-00353) Programs (to S.F.). K.D.K. acknowledges support from the USA National Institutes of Health (GM28962).

Notes and references

1. Tsuji, J. Transition Metal Reagents and Catalysts: Innovations in Organic Synthesis. Wiley; Chichester, U.K.: 2000.
2. (a) Dobereiner GE, Crabtree RH. Chem. Rev. 2010; 110:681. [PubMed: 19938813] (b) Fairlamb IJS. Tetrahedron. 2005; 61:9661.

3. (a) Fagnoni M, Dondi D, Ravelli D, Albini A. Chem. Rev. 2007; 107:2725. [PubMed: 17530909] (b) Oelgemöller M, Jung C, Ortner J, Mattay J, Zimmermann E. Green Chem. 2005; 7:35.
4. (a) Marin ML, Santos-Juanes L, Arques A, Amat AM, Miranda MA. Chem. Rev. 2012; 112:1710. [PubMed: 22040166] (b) Ravelli D, Fagnoni M. ChemCatChem. 2012; 4:169.(c) Ravelli D, Protti S, Neri P, Fagnoni M, Albini A. Green Chem. 2011; 13:1876.
5. (a) Galian RE, Perez-Prieto J. Energy Environ. Sci. 2010; 3:1488.(b) Lewis FD, Bedell AM, Dykstra RE, Elbert JE, Gould IR, Farid S. J. Am. Chem. Soc. 1990; 112:8055.(c) Fox, MA.; Chanon, M. Photoinduced Electron Transfer. Fox, MA., editor. Elsevier; Amsterdam: 1988. p. 1(d) Julliard M, Legris C, Chanon M. J. Photochem. Photobiol., A. 1991; 61:137.
6. (a) Lechner R, Kümmel S, König B. Photochem. Photobiol. Sci. 2010; 9:1367. [PubMed: 20838686] (b) Megerle U, Wenninger M, Kutta R-J, Lechner R, König B, Dickb B, Riedle E. Phys. Chem. Chem. Phys. 2011; 13:8869. [PubMed: 21461426] (c) Svoboda J, Schmaderer H, König B. Chem.–Eur. J. 2008; 14:1854. [PubMed: 18058784] (d) Fukuzumi S, Yasui K, Suenobu T, Ohkubo K, Fujitsuka M, Ito O. J. Phys. Chem. A. 2001; 105:10501.(e) Fukuzumi S, Tanii K, Tanaka T. J. Chem. Soc., Chem. Commun. 1989:816.(f) Fukuzumi S, Kuroda S, Tanaka T. J. Am. Chem. Soc. 1985; 107:3020.
7. (a) Xu H-J, Lin Y-C, Wan X, Yang C-Y, Feng Y-S. Tetrahedron. 2010; 66:8823.(b) Suga K, Ohkubo K, Fukuzumi S. J. Phys. Chem. A. 2003; 107:4339.(c) Ohkubo K, Suga K, Fukuzumi S. Chem. Commun. 2006:2018.(d) Suga K, Ohkubo K, Fukuzumi S. J. Phys. Chem. A. 2005; 109:10168. [PubMed: 16838937] (e) Fukuzumi S, Kuroda S, Tanaka T. J. Chem. Soc., Chem. Commun. 1986:1553.
8. (a) Fukuzumi S. Org. Biomol. Chem. 2003; 1:609. [PubMed: 12929444] (b) Fukuzumi S. Bull. Chem. Soc. Jpn. 2006; 79:177.(c) Fukuzumi S. Phys. Chem. Chem. Phys. 2008; 10:2283. [PubMed: 18414719] (d) Fukuzumi S, Kojima T. J. Mater. Chem. 2008; 18:1427.(e) Fukuzumi S, Ohkubo K. J. Mater. Chem. 2012; 22:4575.
9. (a) Fukuzumi S, Kotani H, Ohkubo K, Ogo S, Tkachenko NV, Lemmetyinen H. J. Am. Chem. Soc. 2004; 126:1600. [PubMed: 14871068] (b) Fukuzumi S, Hanazaki R, Kotani H, Ohkubo K. J. Am. Chem. Soc. 2010; 132:11002. [PubMed: 20698656] (c) Hoshino M, Uekusa H, Tomita A, Koshihara S, Sato T, Nozawa S, Adachi S, Ohkubo K, Kotani H, Fukuzumi S. J. Am. Chem. Soc. 2012; 134:4569. [PubMed: 22375893]
10. Kotani H, Ohkubo K, Fukuzumi S. J. Am. Chem. Soc. 2004; 126:15999. [PubMed: 15584734]
11. Yamada Y, Miyahigashi T, Kotani H, Ohkubo K, Fukuzumi S. J. Am. Chem. Soc. 2011; 133:16136. [PubMed: 21875112]
12. Yamada Y, Miyahigashi T, Kotani H, Ohkubo K, Fukuzumi S. Energy Environ. Sci. 2012; 5:6111.
13. (a) Ohkubo K, Fukuzumi S. Bull. Chem. Soc. Jpn. 2009; 82:303.(b) Kotani H, Ohkubo K, Fukuzumi S. Appl. Catal., B. 2008; 77:317.(c) Ohkubo K, Nanjo T, Fukuzumi S. Catal. Today. 2006; 117:356.(d) Ohkubo K, Yukimoto K, Fukuzumi S. Chem. Commun. 2006:2504.(e) Ohkubo K, Iwata R, Miyazaki S, Kojima T, Fukuzumi S. Org. Lett. 2006; 8:6079. [PubMed: 17165934]
14. Fukuzumi S, Doi K, Suenobu T, Ohkubo K, Yamada Y, Karlin KD. Proc. Natl. Acad. Sci. USA. 2012 DOI: 10.1073/pnas.1119994109.
15. Ohkubo K, Kobayashi T, Fukuzumi S. Angew. Chem., Int. Ed. 2011; 50:8652.
16. Ohkubo K, Kobayashi T, Fukuzumi S. Opt. Express. 2012; 20:A360. [PubMed: 22418686]
17. Ohkubo K, Mizushima K, Fukuzumi Shunichi. Chem. Sci. 2011; 2:715.
18. Ohkubo K, Iwata R, Mizushima K, Souma K, Yamamoto Y, Suzuki N, Fukuzumi S. Chem. Commun. 2010; 46:601.
19. Franz, G.; Sheldon, RA. Ullmann's Encyclopedia of Industrial Chemistry. 5th edn. VCH, Weinheim; Germany: 1991.
20. Sheldon, RA.; Kochi, JK. Metal Catalyzed Oxidation of Organic Compounds. Academic Press; New York: 1981. ch. 10
21. Ballard, RE.; McKillop, A. US. Pat., 4482, 438. 1984.
22. Clarke R, Kuhn A, Okoh E. Chem. Brit. 1975; 11:59.
23. Syper L. Tetrahedron Lett. 1966; 7:4493.
24. Ho T-L. Synthesis. 1973:347.

25. Benniston AC, Elliott KJ, Harrington RW, Clegg W. Eur. J. Org. Chem. 2009; 253

26. (a) Karlin KD, Wei N, Jung B, Kaderli S, Zuberbühler AD. J. Am. Chem. Soc. 1991; 113:5868.(b) Karlin KD, Wei N, Jung B, Kaderli S, Niklaus P, Zuberbühler AD. J. Am. Chem. Soc. 1993; 115:9506.(c) Tyekiar Z, Karlin KD. Acc. Chem. Res. 1989; 22:241.(d) Karlin KD, Kaderli S, Zuberbühler D. Acc. Chem. Res. 1997; 30:139.

27. Weitzer M, Schindler S, Brehm G, Schneider S, Hormann E, Jung B, Kaderli S, Zuberbühler AD. Inorg. Chem. 2003; 42:1800. [PubMed: 12639112]

28. Zhang C, Kaderli S, Costas M, Kim E, Neuhold Y, Karlin KD, Zuberbühler AD. Inorg. Chem. 2003; 42:18073.

29. (a) Smirnov VV, Roth JP. J. Am. Chem. Soc. 2006; 128:3683. [PubMed: 16536541] (b) Jitsukawa K, Harata M, Arii H, Sakurai H, Masuda H. Inorg. Chim. Acta. 2001; 324:108.(c) Harata M, Jitsukawa K, Masuda H, einaga H. J. Am. Chem. Soc. 1994; 116:10817.

30. Wang J, Schopfer MP, Puiu SC, Sarjeant AAN, Karlin KD. Inorg. Chem. 2010; 49:1404. [PubMed: 20030370]

31. Mair RD, Graupner AJ. Anal. Chem. 1964; 36:194.

32. (a) Ohkubo K, Kotani H, Fukuzumi S. Chem. Commun. 2005:4520.(b) Fukuzumi S, Kotani H, Ohkubo K. Phys. Chem. Chem. Phys. 2008; 10:5159. [PubMed: 18701967]

33. Fukuzumi S, Suenobu T, Patz M, Hirasaka T, Itoh S, Fujitsuka M, Ito O. J. Am. Chem. Soc. 1998; 120:8060.

34. (a) Fukuzumi S, Patz M, Suenobu T, Kuwahara Y, Itoh S. J. Am. Chem. Soc. 1999; 121:1605.(b) Kawashima T, Ohkubo K, Fukuzumi S. Phys. Chem. Chem. Phys. 2011; 13:3344. [PubMed: 21212887]

35. Fukuzumi S, Kotani H, Lucas HR, Doi K, Suenobu T, Peterson R, Karlin KD. J. Am. Chem. Soc. 2010; 132:6874. [PubMed: 20443560]

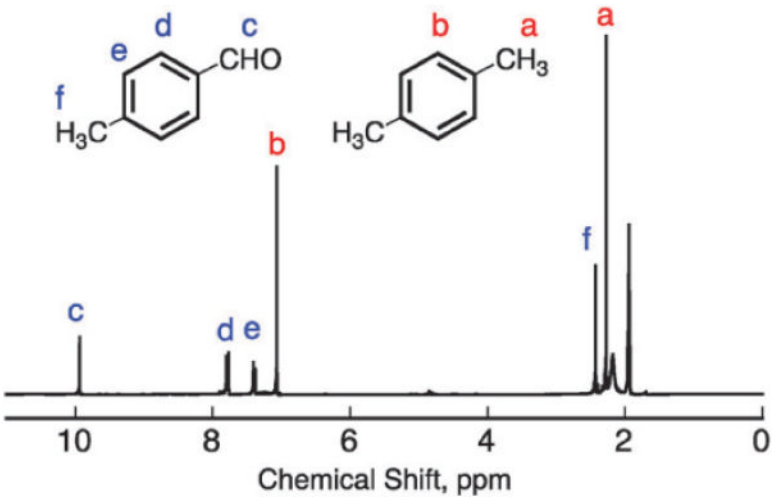

Fig. 1.

A ^{1}H NMR spectrum of oxygen-saturated CD_3CN solution containing Acr^{+}–Mes (2.0×10^{-4} M), $[(tmpa)Cu^{II}]^{2+}$ (1.0×10^{-3} M) and *p*-xylene (3.0×10^{-2} M) after photoirradiation for 3.5 h. The peaks labelled a and b were assigned to *p*-xylene and those labelled c–f were due to *p*-tolualdehyde.

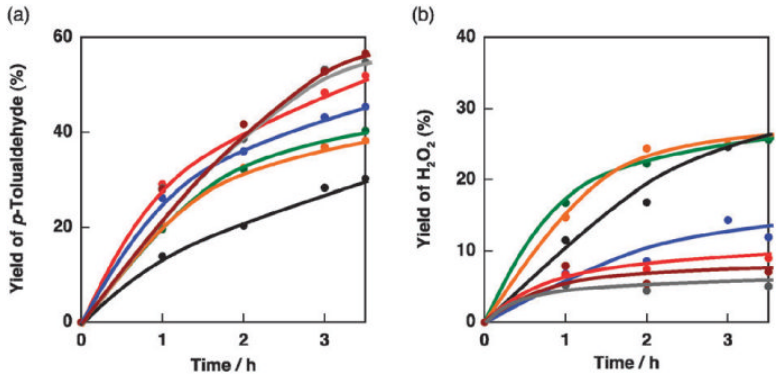

Fig. 2.

(a) Time profiles of the yield of *p*-tolualdehyde in the photo-oxygenation of *p*-xylene (3.0×10^{-2} M) in oxygen-saturated CD_3CN containing Acr^+–Mes (2.0×10^{-4} mM) and $[(tmpa)Cu^{II}]^{2+}$ (0–3.0 mM). (b) Time profiles of the yield of H_2O_2 in the photooxygenation of *p*-xylene (3.0×10^{-2} M) in oxygen-saturated CD_3CN containing Acr^+–Mes (2.0×10^{-4} M) and $[(tmpa)Cu^{II}]^{2+}$ (0 mM, black; 0.05 mM, orange; 0.10 mM, green; 0.5 mM, blue; 1.0 mM, red; 2.0 mM, grey and 3.0 mM, brown).

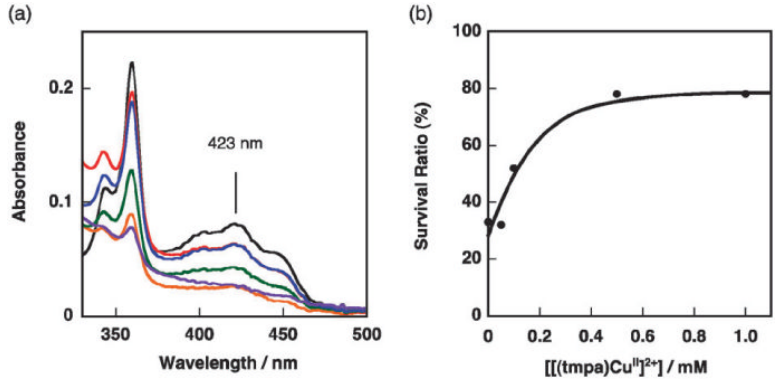

Fig. 3.

(a) UV-vis spectra of reaction solutions after photoirradiation for 3.5 h. ([Acr–Mes]: 2.0×10^{-4} M, [(tmpa)Cu^{II}]$^{2+}$: 0 mM, black; 0.05 mM, orange; 0.10 mM, green; 0.5 mM, blue; 1.0 mM, red; 2.0 mM). (b) The survival ratio of Acr^{+}–Mes after photoirradiation for 3.5 h as a function of the concentration of [(tmpa)Cu^{II}]$^{2+}$.

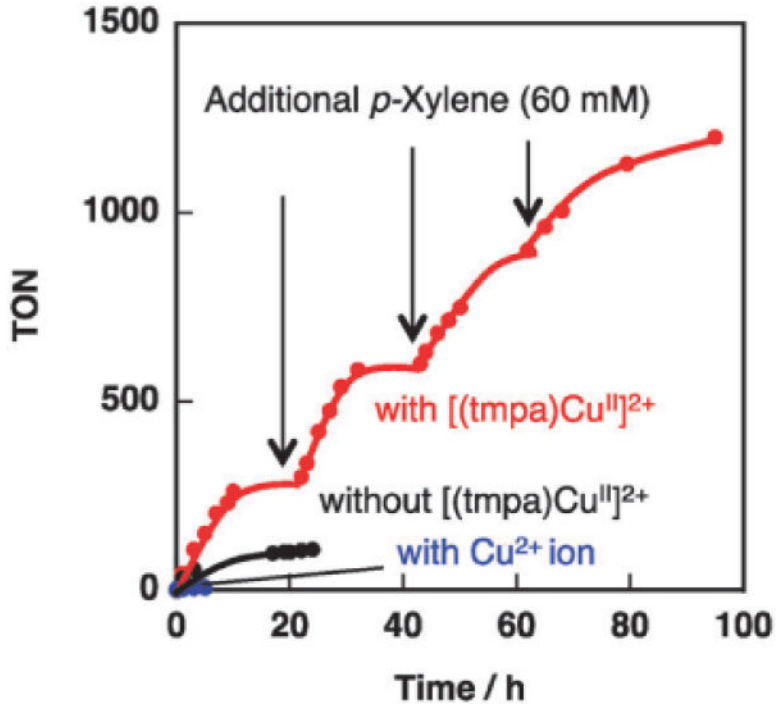

Fig. 4.

Time profiles of the turnover number for *p*-xylene oxygenation (6.0×10^{-2} M) under photoirradiation ($\lambda > 390$ nm) of an O_2-saturated MeCN solution containing Acr^+–Mes (2.0×10^{-4} M) in the absence or presence of $[(tmpa)Cu^{II}]^{2+}$ or $Cu(ClO_4)_2$ (2.0×10^{-3} M). TON = [oxygenated products]/[Acr^+–Mes].

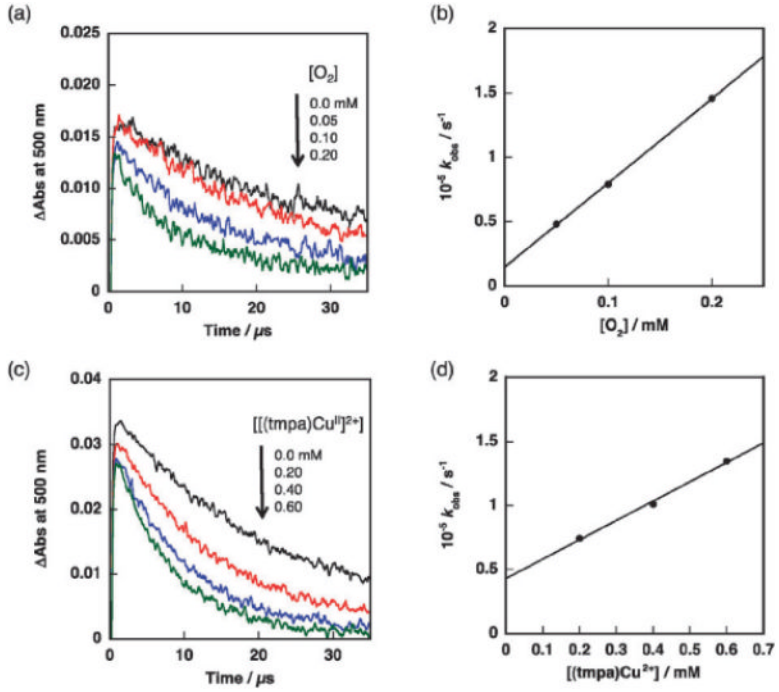

Fig. 5.

(a) Transient absorbance time profiles at 500 nm due to $Acr^{\cdot}$–$Mes^{\cdot}$ in CH_3CN containing Acr^+–Mes (1.0×10^{-4} M) and oxygen (0 to 2.0×10^{-4} mM) after laser irradiation (λ = 430 nm). (b) A plot of the pseudo-first-order rate constant (k_{obs}) for electron transfer from the $Acr^{\cdot}$ moiety of $Acr^{\cdot}$–$Mes^{\cdot+}$ to O_2 *vs.* [O_2]. (c) Time profiles of absorbance at 500 nm due to $Acr^{\cdot}$–$Mes^{\cdot+}$ in CH_3CN containing Acr^+–Mes (1.0×10^{-4} M) and $[(tmpa)Cu^{II}]^{2+}$ (0 to 6.0×10^{-4} mM) after photoirradiation (λ = 430 nm). (d) A plot of the pseudo-first-order rate constant (k_{obs}) for electron transfer from the $Acr^{\cdot}$ moiety of $Acr^{\cdot}$–$Mes^{\cdot+}$ to $[(tmpa)Cu^{II}]^{2+}$ *vs.* $[[(tmpa)Cu^{II}]^{2+}]$.

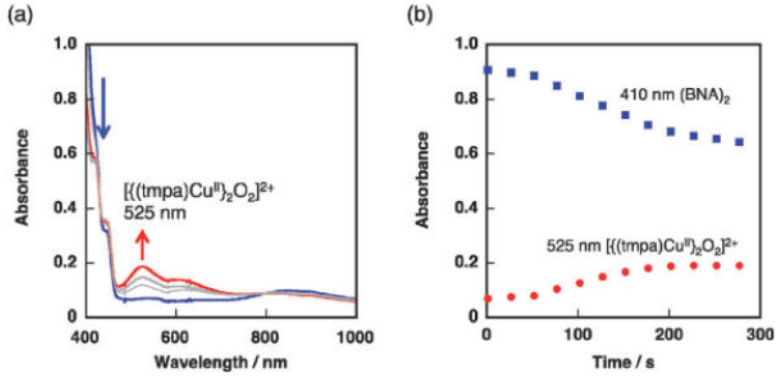

Fig. 6.

(a) The UV-vis spectral change of an EtCN solution containing $(BNA)_2$ (2.5×10^{-4} M), Acr^+–Mes (5.0×10^{-5} M) and $[(tmpa)Cu^{II}]^{2+}$ (5.0×10^{-4} M) before (blue line) and after (red line) photoirradiation (λ = 420 nm) at 203 K. (b) Time profiles of absorbance at 410 nm due to $(BNA)_2$ (blue square) and 525 nm due to $[\{(tmpa)Cu^{II}\}_2O_2]^{2+}$ complex (red circle).

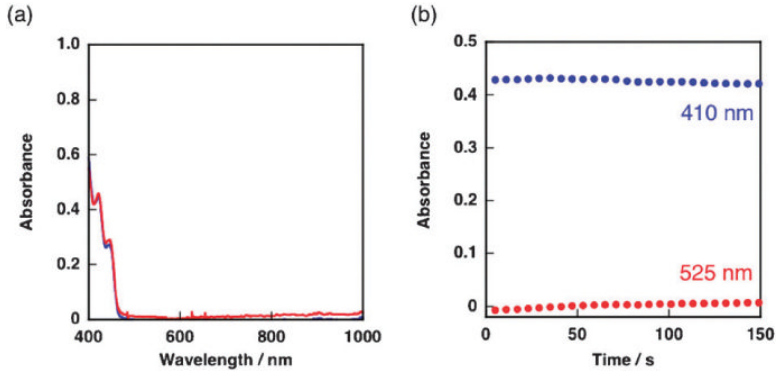

Fig. 7.

(a) The UV-vis spectral change of an EtCN solution containing $(BNA)_2$ (2.5×10^{-4} M), Acr^+–Mes (5.0×10^{-5} M) and $Cu^{II}(ClO_4)_2$ (5.0×10^{-4} M) before (blue line) and after (red line) photoirradiation (λ = 420 nm) at 203 K. (b) Time profiles of absorbance at 410 nm due to $(BNA)_2$ (blue circle) and 525 nm due to dimeric copper species (red circle).

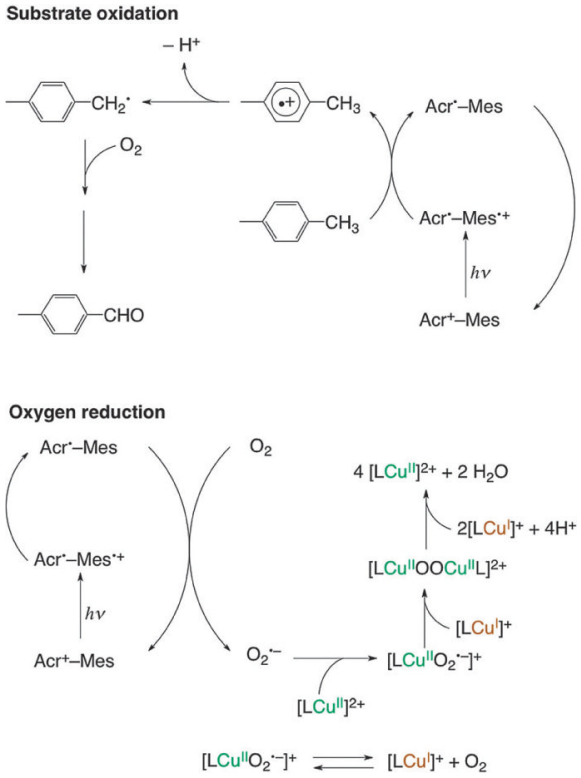

Scheme 1.

The reaction mechanism of the photocatalytic oxygenation of *p*-xylene with O_2 in the presence of $[(tmpa)Cu^{II}]^{2+}$. (L = tmpa).